JBC Papers in Press. Published on September 22, 2015 as Manuscript M115.682179
The latest version is at http://www.jbc.org/cgi/doi/10.1074/jbc.M115.682179

Cytosolic Fe-S Cluster Protein Maturation and Iron Regulation Are Independent of the Mitochondrial Erv1/Mia40 Import System

Hatice K. Ozer[‡,1], Adrienne C. Dlouhy[‡,1], Jeremy D. Thornton[§], Jingjing Hu[‡], Yilin Liu[#], Joseph J. Barycki[#], Janneke Balk[§], and Caryn E. Outten[‡,*]

[‡]Department of Chemistry and Biochemistry, University of South Carolina, Columbia, South Carolina, USA
[§]John Innes Centre and University of East Anglia, Norwich Research Park, Norwich, U.K.
[#]Department of Biochemistry and the Redox Biology Center, University of Nebraska, Lincoln, Nebraska, USA

Running Title: *Yeast Iron Metabolism is Independent of Erv1/Mia40 Function*

[1]These authors contributed equally to this work.

*Corresponding author address: Dr. Caryn E. Outten, University of South Carolina, 631 Sumter St., Columbia, SC 29208 USA, Tel: +1-803-777-8783; Fax: +1-803-777-9521; E-mail: outten@mailbox.sc.edu

Keywords: Iron metabolism, glutathione, iron-sulfur protein, mitochondrial transport, sulfhydryl oxidase

Background: The mitochondrial sulfhydryl oxidase Erv1 is implicated in cytosolic iron-sulfur protein maturation and iron regulation.
Results: An *erv1* yeast strain used in previous iron metabolism studies is glutathione-deficient, and *erv1/mia40* mutants with sufficient glutathione do not exhibit iron-related defects.
Conclusion: Iron homeostasis is independent of Erv1/Mia40 function.
Significance: The unexplained role of Erv1 in yeast iron metabolism is resolved.

ABSTRACT

The sulfhydryl oxidase Erv1 partners with the oxidoreductase Mia40 to import cysteine-rich proteins in the mitochondrial intermembrane space. In *Saccharomyces cerevisiae*, Erv1 has also been implicated in cytosolic Fe-S protein maturation and iron regulation. To investigate the connection between Erv1/Mia40-dependent mitochondrial protein import and cytosolic Fe-S cluster assembly, we measured Mia40 oxidation and Fe-S enzyme activities in several *erv1* and *mia40* mutants. While all the *erv1* and *mia40* mutants exhibited defects in Mia40 oxidation, only one *erv1* mutant strain (*erv1-1*) had significantly decreased activities of cytosolic Fe-S enzymes. Further analysis of *erv1-1* revealed that it had strongly decreased glutathione (GSH) levels, caused by an additional mutation in the gene encoding the glutathione biosynthesis enzyme glutamate cysteine ligase (*GSH1*). To address whether Erv1 or Mia40 plays a role in iron regulation, we measured iron-dependent expression of Aft1/2-regulated genes and mitochondrial iron accumulation in *erv1* and *mia40* strains. The only strain to exhibit iron misregulation is the GSH-deficient *erv1-1* strain, which is rescued with addition of GSH. Together, these results confirm that GSH is critical for cytosolic Fe-S protein biogenesis and iron regulation, while ruling out significant roles for Erv1 or Mia40 in these pathways.

Erv1 is an FAD-dependent sulfhydryl oxidase localized to the mitochondrial intermembrane space (IMS)[1]. Erv1 has an essential, well-established role in importing small, cysteine-containing proteins into the IMS via a disulfide relay with the import receptor Mia40 (1,2).

[1]Abbreviations: IMS, intermembrane space; ISC, iron-sulfur cluster; CIA, cytosolic iron-sulfur cluster assembly; GS-S-SG, glutathione polysulfide; SC, synthetic complete; PMS, post-mitochondrial supernatant; NEM, *N*-ethylmaleimide; BPS, bathophenanthroline disulfonate

Substrate proteins for this pathway enter the IMS in an unfolded reduced state, where Mia40 catalyzes oxidation of cysteine pairs in the imported proteins, facilitating their folding and retention in the IMS (3,4). Erv1 catalyzes reoxidation of Mia40 and shuttles the electrons to the respiratory chain (5,6). The substrate proteins of the Mia40-Erv1 pathway play critical roles in mitochondrial protein import, assembly of respiratory chain components, and removal of reactive oxygen species. As such, defects in Mia40 or Erv1 lead to depletion of these IMS proteins causing a variety of phenotypes, including respiratory deficiency, loss of mitochondrial DNA, and aberrant mitochondrial morphology. The importance of this pathway is highlighted by the fact that yeast deletion mutants for *ERV1* and *MIA40* are inviable (6).

In addition to participating in IMS protein import, Erv1 was suggested to have a role in exporting a sulfur-containing compound from the mitochondrion to the cytosol required for maturation of cytosolic Fe-S cluster proteins and regulation of iron homeostasis (7,8). The mitochondrion houses the iron-sulfur cluster (ISC) pathway for Fe-S cluster assembly, which is required not only for the biogenesis of Fe-S containing proteins in the mitochondria, but also for cytosolic and nuclear Fe-S proteins (8). The maturation of most Fe-S proteins in the cytosol and nucleus relies on the CIA (cytosolic iron-sulfur protein assembly) machinery (9). The connection between the ISC and CIA assembly pathways is thought to occur via export of a sulfur-containing compound from the mitochondrial matrix to the cytosol that is used to build and/or insert Fe-S clusters into cytosolic proteins. This compound is a product of the ISC pathway and is exported by the ATP binding cassette transporter Atm1 (10). One of the substrates for Atm1 was recently identified as glutathione polysulfide (GS-S-SG), suggesting that the thiol-containing tripeptide glutathione (GSH) helps transport an activated persulfide (S^0) from the mitochondria to the cytosol for Fe-S cluster assembly (11). This finding is supported by the recent crystal structures of yeast Atm1 and its bacterial homologue with bound GSH and/or GSSG (12,13). The ISC pathway, Atm1, and GSH also impact on activity of the iron-responsive transcriptional regulators Aft1 and Aft2 (14-16). In the proposed regulation model, the substrate exported by Atm1 is used to assemble Fe-S clusters on the cytosolic glutaredoxins Grx3 and Grx4, which use GSH to coordinate the Fe-S clusters and help deliver them to Aft1 and Aft2. In turn, Fe-S cluster binding by Aft1 and Aft2 inhibits their ability to bind to and activate iron uptake and mobilization genes (17,18).

Erv1's putative role in this regulation pathway and in the maturation of cytosolic Fe-S cluster proteins stems from a single report in which a temperature-sensitive *erv1* mutant strain (*erv1-1*) displayed Fe-S related phenotypes similar to strains depleted of GSH or Atm1 (7,19-21). These phenotypes included diminished iron incorporation into two cytosolic Fe-S proteins, Leu1 and Rli1, and accumulation of mitochondrial iron caused by dysregulation of iron homeostasis. Based on these results, it was suggested that the IMS-localized protein Erv1 functions together with Atm1 and GSH to export the mitochondrial ISC-derived substrate required for cytosolic Fe-S cluster assembly and iron sensing (8).

Since the specific role of Erv1 in cytosolic Fe-S cluster biogenesis and iron metabolism was unclear, we analyzed Fe-S protein activity in a number of *erv1* mutant strains. Furthermore, we extended our studies to include *mia40* mutants to determine whether Erv1's role in these iron pathways is linked to its disulfide relay function with Mia40. Surprisingly, we discovered that the *erv1-1* strain originally tested for Fe-S cluster defects by Lange and coworkers (7) was the only strain to exhibit defects in the cytosolic Fe-S enzymes isopropylmalate isomerase and sulfite reductase. Mitochondrial and cytosolic Fe-S enzyme activities in the other *erv1* and *mia40* mutants tested were similar to or higher than the WT control. We found that the *erv1-1* strain had dramatically depleted GSH levels in both the mitochondria and cytosol, while GSH levels were normal in other *erv1* and *mia40* mutants. The cause of GSH deficiency in the *erv1-1* strain was a previously undetected mutation in the *GSH1* gene encoding glutamate cysteine ligase, which catalyzes the first step in GSH biosynthesis. Addition of GSH to the growth media rescued both the sulfite reductase activity and iron regulation. These results demonstrate that the defects in cytosolic Fe-S enzymes and iron homeostasis in *erv1-1* are due to GSH depletion.

Taken together, these results indicate that neither Erv1 nor Mia40 play significant roles in cytosolic Fe-S cluster assembly and iron homeostasis.

MATERIALS AND METHODS

Yeast Strains, Media, and Growth Conditions—*S. cerevisiae* strains used in this study are listed in Table 1. Temperature-sensitive strains were grown overnight at 24 ºC on synthetic complete (SC) medium supplemented with 2% glucose and the appropriate amino acids. One set was then diluted, shifted to 37 °C, and grown for 5 more hrs while the other set was diluted and maintained at 24 °C. *GAL*-regulated strains were maintained at 30 °C on SC medium in the presence of 2% raffinose + 0.5% galactose to induce expression or grown in 2% raffinose for at least 64 hrs to repress expression. For plasmid shuffling, an *erv1* deletion strain with wild-type Erv1 expressed on a *URA3* plasmid (Spore 2A) was transformed with a *TRP1* plasmid carrying Erv1(F124S) (pYX232-*erv1*(F124S) described below). Transformants were selected on SC-Trp plates and shuffling of the *URA3*-marked plasmid expressing WT Erv1 was carried out with 5-fluoroorotic acid. Yeast transformations were performed by the lithium acetate procedure. All assays were performed on strains at mid-log phase.

Construction of Plasmids—The 2μ *TRP1* plasmid pYX232-*erv1*(F124S) was generated by site-directed mutagenesis of pYX232-*ERV1* (22)) using the QuikChange II Mutagenesis kit (Agilent). The *CEN LEU2* plasmid p415-ADH-GSH1 was constructed by insertion of the *GSH1* open reading frame in the XbaI and XhoI sites of p415-ADH ((23). A triple tandem HA epitope was incorporated at the C-terminus of Gsh1 at an engineered NotI site. All plasmid inserts were verified by DNA sequencing.

Subcellular Fractionation—Yeast cells were grown aerobically to mid-log phase in selective SC medium with 2% glucose. Mitochondrial and post-mitochondrial supernatant (PMS) fractions were obtained as previously described by converting cells to spheroplasts followed by gentle lysis by Dounce homogenization and differential centrifugation (24). Incubation with DTT was omitted from the spheroplasting step to avoid perturbation of the intracellular thiol redox state. Protein concentrations in extracts were determined using the Bradford method (Bio-Rad) with bovine serum albumin as the calibration standard.

Glutathione Assay—Total glutathione (GSH + GSSG) in PMS and mitochondrial extracts was measured by the DTNB-GSSG reductase recycling assay as described previously (25) or the GSH/GSSG-Glo™ Assay following the manufacturer's protocol with slight modifications (Promega). For whole cell GSH measurements, 1-4×10^5 cells (or 0.5-1×10^7 for *erv1-1* strains) were harvested by centrifugation, resuspended in lysis buffer supplied by the GSH/GSSG-Glo™ Assay kit, and lysed via mechanical disruption with glass beads. After addition of luciferin generation and detection reagents, stable luciferin luminescent signals were detected using the Synergy H1 Hybrid Multi-Mode Microplate Reader (Biotek, USA). The results are expressed as nmoles GSH per 10^7 cells (assuming 1 OD_{600} = 2×10^7 cells).

Non-reducing SDS-PAGE—Non-reducing SDS-PAGE was performed as previously described (26). Briefly, cells were grown in SC media to mid-log phase and then acid-quenched with TCA (Sigma) (15% (w/v) final concentration) at 4 °C for 20 min. Five OD_{600} units of cells were harvested by centrifugation and resuspended in 1 ml of 10% TCA. Following glass bead lysis, lysed cells were transferred to a new tube and pelleted by centrifugation. The pellet was resuspended in 500 μl of 1× non-reducing SDS sample buffer containing 40 mM *N*-ethylmaleimide (NEM) (Sigma). Following a 10-min incubation at room temperature, proteins were separated on 16% Tris-glycine gels (Invitrogen). Reduced and oxidized forms of Mia40 were analyzed by quantitative immunoblot using an Odyssey Infrared Imaging System (LI-COR).

Immunoblotting Techniques—Yeast extracts subjected to gel electrophoresis were analyzed by Western blotting using anti-Erv1 or anti-Mia40 antibodies (both kind gifts of J. Riemer) or anti-Gsh1 antibodies using a secondary anti-rabbit IgG (IRDye, LI-COR, Lincoln, NE). Recombinant yeast Gsh1 was produced in *E. coli* as described previously (27) and the purified enzyme was used to produce a rabbit anti-Gsh1 antibody (Covance). Human IRP1 antibody was purchased from Santa

Cruz Biotechnology. Cytosolic and mitochondrial fractions were monitored by anti-phosphoglycerate kinase (PGK1) and anti-porin antibodies (Invitrogen), respectively, using a secondary anti-mouse IgG (IRDye, LI-COR, Lincoln, NE). Western blots were visualized and quantified using an Odyssey Infrared Imaging System (LI-COR).

GSH1 Gene Sequencing—Genomic DNA for JRY-675 and *erv1-1* strains was isolated using the Promega Wizard Genomic DNA Purification Kit and the *GSH1* gene amplified from –720 to +2380 by PCR using primers listed in Table 2. The purified DNA fragments were subjected to Sanger sequencing at the Selah Clinical Genomics Center at Innovista (Columbia, SC).

RNA Isolation and Quantitative Real-Time PCR (qRT-PCR)—Total RNA was isolated from yeast strains JRY-675 and *erv1-1* with the PureLink RNA Mini kit (Invitrogen) following the manufacturer's protocol. Yeast RNAs were reverse transcribed into cDNAs with the SuperScript III First-Strand Synthesis System (Invitrogen) following the manufacturer's recommendations. Using the primers shown in Table 2, qRT-PCR was carried out on an IQ ICycler (Biorad) with the RT^2 SYBR Green Fast Mastermix (Qiagen). The relative quantification of *GSH1* expression was calculated by the $2^{-\Delta\Delta C_T}$ method (28) using the *ACT1* gene (actin) as a control.

Cytosolic Fe-S cluster Enzyme Activity Assays—For Leu1 (isopropylmalate isomerase) assays, temperature-sensitive strains and corresponding parent strains were grown in SC-glucose media at 24 °C until OD_{600} 1 – 1.5. The OD_{600} was adjusted to 1.0 and cells were incubated at 37 °C for 5 hours with or without 1 mM GSH. Yeast cells were harvested, washed and broken with glass beads in TNETG buffer (20 mM Tris-HCl pH 7.4, 2.5 mM EDTA, 150 mM NaCl, 10% (v/v) glycerol, 0.5% (w/v) Triton X-100). Cell debris was removed by centrifugation. Leu1 enzyme activity was measured as the conversion of 2-isopropylmaleate to 2-isopropylmalate at 235 nm. As an indirect assay for sulfite reductase, yeast cells were plated on bismuth sulfite ($Bi_2(SO_3)_3$) plates and incubated at 30 °C for 48 hrs. Reduction of sulfite (SO_3^{2-}) to sulfide (S^{2-}) results in formation of bismuth sulfide (Bi_2S_3) as a brown precipitate. 1 mM GSH was included in the plates where indicated.

In-Gel Aconitase Activity Assay—Cytosolic and mitochondrial aconitase activities were monitored using an in-gel activity assay described previously (29). We note that these assays were performed in cells with a complete leucine biosynthetic pathway since the *LEU2* IRP1 plasmid was selected for in media lacking leucine. Thus, aconitase activity should be unaffected by increased expression of Leu1 as occurs in *leu2*Δ strains, which subsequently impacts Fe-S delivery to aconitase (30,31). Yeast cells expressing human cytosolic aconitase IRP1 from pRS425-IRP1 (YEp-*LEU2*) were grown to mid-log phase in selective SC media, harvested and washed with sterile water. The pellets were then resuspended in lysis buffer (50 mM Tris-HCl, pH 8.0, 10% glycerol, 50 mM NaCl, 2.5% Triton X-100, 0.5 mM PMSF, 1 mM DTT, 2 mM citrate, protease inhibitor cocktail, 200 U/ml catalase) and subjected to glass bead lysis. Extracts were centrifuged and the supernatants were collected for assaying. Protein concentration of the extracts was determined by the Bradford method (Bio-Rad). A chilled 8% Tris-borate-citrate polyacrylamide gel was pre-electrophoresed in Tris-glycine-citrate running buffer at 140 V for 40 min. Subsequently, 100 µg of protein was loaded to the gel and electrophoresed at 140 V for 3.5 hours on ice. Gels were incubated at 37 °C for 30 min in the dark with aconitase activity assay stain (100 mM Tris-HCl, pH 8.0, 1 mM $NADP^+$, 2.5 mM cis-aconitate, 5 mM $MgCl_2$, 1.2 mM methylthiazolyldiphenyl-tetrazolium bromide, 0.3 mM phenazine methosulfate, and 5 U/ml isocitrate dehydrogenase) and scanned.

β-galactosidase Assays—All strains tested were transformed with the *FET3*-LacZ reporter construct pFC-W (YEp-*URA3*) that contains the *FET3* iron-response element in a minimal promoter (32) or the *FIT3-LacZ* reporter construct p*FIT3-LacZ* (YEp-*URA3*) that contains the *FIT3* promoter (33). Temperature-sensitive *erv1*, *mia40*, and corresponding parent strains were grown in selective SC glucose media at 24 °C to an OD_{600} of 1 and then divided into 3-ml aliquots for induction. The cultures were incubated at 24

and 37 °C with either 50 μM $FeCl_3$ (high Fe), 100 μM bathophenanthroline disulfonate (BPS) (low Fe), or no addition (normal Fe) for 5 hours. *GAL-ERV1* and the parent W303A strain were grown for 64 hours at 30 °C to an OD_{600} of 1 in inducing (SC-raffinose/galactose) or repressing (SC-raffinose) media and were similarly divided into high, low, and normal Fe aliquots and grown for an additional 4 hours at 30 °C. Cells were then harvested and assayed for β-galactosidase activity as previously described (34).

Intracellular Iron Analysis—Mitochondrial and cytosolic iron content was measured using atomic absorption spectroscopy. Yeast cells were grown to mid-log phase in SC glucose media for temperature-sensitive strains, or SC galactose/raffinose for W303A, *GAL-ERV1* and *GAL-ATM1* strains, and mitochondria and PMS fractions were prepared as described above. Extracts were diluted in Milli-Q water and iron analysis of fractions was performed on a PerkinElmer PinAAcle 900T graphite furnace atomic absorption spectrometer using the manufacturer's recommended conditions.

Data Analysis—For all assays and quantifications, averages and standard deviations were calculated from at least three independent experiments.

RESULTS

The erv1-1 strain but not other erv1 mutants exhibits cytosolic Fe-S protein defects. To better understand the connection between Erv1 function and cytosolic Fe-S cluster biogenesis, we obtained several different *erv1* mutants. The temperature-sensitive *erv1* strain (*pet492-6A*), named *erv1-1*, was first described by Lisowsky (19,35), and shown to exhibit defects in IMS protein import (4) and maturation of cytosolic Fe-S clusters (7). This strain harbors an Erv1 F124S mutation located at the dimer interface (36) and therefore likely impairs Erv1 dimerization, which is essential for catalytic function (22). The *erv1-2* and *erv1-5* strains each contain single point mutations in the *ERV1* gene creating N166D and C159S substitutions, respectively (37). Asn-166 and Cys-159 are both located near the FAD binding site, with Cys-159 forming a structural disulfide with Cys-176 (36). As such, the C159S Erv1 mutant exhibits decreased FAD binding *in vitro* (38), while both *erv1-2* and *erv1-5* are impaired in import of IMS proteins (3,37,39). We confirmed the Erv1 functional defect by assessing the *in vivo* redox state of the import receptor Mia40 at the permissive (24 °C) and restrictive (37 °C) temperatures. As expected, the redox-active cysteine pair in Mia40 is ~88% oxidized in both the WT and *erv1-1* strains at 24 °C, but is only ~33% oxidized in *erv1-1* at 37 °C (Fig. 1, left). The defect in Mia40 oxidation is similar to that found in the *erv1-2* and *erv1-5* strains (Fig. 1, right).

Consistent with the report by Lange et al. (7), the *erv1-1* strain exhibited a 40% decrease in the activity of isopropylmalate isomerase (Leu1) compared to the genetically-matched WT strain (Fig. 2A). This decrease, however, was not as severe as measured for the temperature-sensitive *nbp35-1* strain (~90% activity loss), which is known to be defective in cytosolic Fe-S cluster protein maturation (40,41). Leu1 protein levels were similar for *erv1-1, nbp35-1* and their respective wild-types (Fig. 2B), thus differences in protein synthesis did not cause the Fe-S enzyme defects in *erv1-1* or *nbp35-1*. In order to test whether the Fe-S defect in the *erv1-1* strain is linked to the Erv1-Mia40 mitochondrial import system, we measured Leu1 activity in other *erv1* and *mia40* temperature-sensitive strains. Leu1 activity was actually increased in the *erv1-2* and *erv1-5* strains compared to the WT control (Fig. 2A). Similarly, Leu1 activity measured for *mia40-3* was comparable to WT. We further measured sulfite reductase activity, another cytosolic [4Fe-4S]-dependent enzyme, using a bismuth sulfite plate assay in which the sulfide product reacts with bismuth to give a brown color. As shown in Figure 2C (left panel), the *erv1-1* strain exhibited a marked defect in sulfite reductase activity. We note that sulfite reductase activity could not be assessed for the *erv1-2* and *erv1-5* alleles using this assay, because the strains were unable to grow on bismuth plates for unknown reasons. Since GSH and Erv1 are proposed to function together in cytosolic Fe-S cluster assembly, we tested whether GSH addition influenced Fe-S activity in the *erv1-1* mutant. Interestingly, addition of 1 mM GSH to the growth media rescued the sulfite reductase defect in this strain (Fig. 2C, right panel).

As a complementary approach to examine the role of Erv1 in Fe-S cluster assembly, we

expressed human IRP1 in the yeast cytosol, which acts as a cytosolic Fe-S assembly reporter (42-44). The Fe-S-dependent aconitase activities of IRP1 and the native yeast mitochondrial aconitase (Aco1) were then assessed in parallel via an in-gel activity assay (29). Both aconitase activities were very low in the WT(1) and *erv1-1* strain (Fig. 2D). However, addition of 1 mM GSH to the growth medium increased cytosolic aconitase activity in the *erv1-1* mutant at both 24 (permissive) and 37 °C (restrictive temperature) with little effect on the WT control. In addition, we tested aconitase activity in the *erv1-2, erv1-5*, *mia40-3*, and *mia40-4* mutants in the YPH499 background (Fig. 4E). Although these assays display some variability from one data set to another, none of these mutants showed any clear difference in cytosolic or mitochondrial aconitase activity when compared to WT controls at either 24 or 37 °C. Furthermore, addition of GSH did not influence the observed aconitase activities in these strains (data not shown). Taken together, these data suggest that Fe-S cluster defects are unique to the *erv1-1* mutant and argue against a major role for either Erv1 or Mia40 in the maturation of cytosolic Fe-S cluster proteins.

Cytosolic and mitochondrial GSH pools are depleted in *erv1-1* but not in other *erv1* or *mia40* mutant strains. Since GSH addition increased Fe-S enzyme activity in the *erv1-1* strain, we measured endogenous GSH levels in this mutant. Surprisingly, the *erv1-1* strain exhibited strongly decreased levels of GSH at both 24 and 37 °C (Fig. 3A, left), as compared to the WT control. We further fractionated yeast cells into mitochondrial and cytosolic extracts to determine whether the GSH deficiency impacted these specific compartments differently. We measured a ~30-fold decrease in cytosolic GSH levels in the *erv1-1* strain compared to WT at 24 °C that further decreased to ~120-fold at 37 °C (Fig. 3B, left). In the mitochondria, the differences were less extreme since the GSH levels in *erv1-1* were ~7-fold lower that WT at 24 °C and ~80-fold lower at 37 °C (Fig. 3C, left).

In order to test whether the GSH depletion phenotype discovered in the *erv1-1* strain is directly related to the Erv1-Mia40 import system or unique to that specific mutant, we measured total GSH levels in the other *erv1* and *mia40* temperature-sensitive strains we obtained (3,37,39). Total GSH levels in whole cell, mitochondrial, and cytosolic extracts for these *erv1* and *mia40* strains were similar to the WT control (Fig. 3A-C, right panels). To investigate whether the GSH depletion phenotype is related to changes in Erv1 protein levels, we performed Erv1 immunoblot analysis for these strains. Erv1 expression levels in mitochondrial fractions consistently decreased at 37 °C for all *erv1* and *mia40* mutants tested, including *erv1-1* (Fig. 3D). This result is expected given that Erv1 itself is a substrate of the Erv1-Mia40 import pathway, and thus its import into the IMS is impaired with disruption of either Erv1 or Mia40 function (45). However, the data indicate that alterations in Erv1 protein levels do not correlate with GSH deficiency in these temperature-sensitive mutants. We next questioned whether the specific Erv1 mutation harbored by the *erv1-1* strain is the cause of the GSH defect. The *erv1-1* mutation (F124S) was recreated in the W303A strain background by plasmid shuffling. This *erv1*(F124S) strain exhibited a defect in Mia40 oxidation at the restrictive temperature confirming Erv1 dysfunction (Fig. 4A,B left); however, total GSH levels were similar to WT at both temperatures (Fig. 4C, left). From these results we conclude that the Erv1 F124S mutation is not the cause of GSH deficiency in the *erv1-1* strain.

To further understand how changes in Erv1 expression influence GSH levels independent of temperature effects, we measured total GSH levels in a *GAL*-regulated *ERV1* strain that allows Erv1 overexpression or depletion depending on the presence or absence of galactose in the growth media (Fig. 4A, right). Increased expression of Erv1 led to a more oxidized *in vivo* redox state for Mia40, while decreased expression led to a more reduced state (Fig. 4A,B right), as previously reported (6). Interestingly, both overexpression and depletion of Erv1 resulted in a 2- to 3-fold increase in total GSH levels compared to the WT control (Fig. 4C, right), rather than a severe decrease as measured for the *erv1-1* strain. Taken together, these results demonstrate that GSH deficiency is unique to the *erv1-1* strain, unrelated to Erv1 protein levels, and not a general phenotype of Erv1 or Mia40 dysfunction.

***erv1-1* has markedly decreased Gsh1 protein levels due to a mutation in *GSH1*.** To uncover the origin of the GSH deficiency in *erv1-1*, we tested for defects in the GSH biosynthetic pathway in this strain. The tripeptide GSH (γ-glutamylcysteinyl glycine) is synthesized in two steps via glutamate cysteine ligase (Gsh1) and GSH synthase (Gsh2). Gsh1 forms the linkage between glutamate and cysteine, while Gsh2 catalyzes the addition of glycine. Addition of cysteine, glycine or glutamate to the growth media did not rescue the GSH deficiency in the *erv1-1* strain (data not shown), suggesting that the GSH defect is not due to a lack of these GSH precursors. We next tested for changes in expression of the first biosynthetic enzyme, glutamate cysteine ligase (Gsh1). Interestingly, the *erv1-1* strain has strongly decreased Gsh1 protein levels compared to WT controls and other *erv1* and *mia40* mutants at both 24 and 37 °C (Fig. 5A,B). However, *GSH1* RNA levels were consistently higher in the *erv1-1* strain (Fig. 5C) compared to WT, ruling out a transcriptional or post-transcriptional defect. Therefore, we sequenced the *GSH1* gene in the *erv1-1* strain to determine whether the decrease in Gsh1 levels is due to a mutation in the *GSH1* open reading frame. A G-to-A mutation was discovered at +839 in the coding sequence, changing an Arg at position 280 to His (Fig. 5D). Arg-280 is well-conserved across eukaryotic Gsh1 protein sequences (Fig. 5D). It forms a salt bridge with Asp-403 (Fig. 5E) as well as backbone hydrogen bonds with Leu-369 and Gly-370. Disruption of these interactions may impact the placement of Tyr-362 (in a loop region) which helps coordinate the alpha-carboxylate of the glutamate substrate (27). Thus, the R280H mutation likely affects both the enzymatic activity and the protein stability of glutamate cysteine ligase (Fig. 5E). Expressing WT *GSH1* on a plasmid or adding GSH to the culture medium rescues the GSH deficiency phenotype (Fig. 6A,B). Taken together, these results demonstrate that GSH deficiency in *erv1-1* is caused by a previously undetected mutation in the gene encoding glutamate cysteine ligase (*GSH1*).

Defects in iron regulation in erv1-1 are rescued by GSH. In addition to exhibiting cytosolic Fe-S cluster deficiency, mutations in *erv1* have also been implicated in dysregulation of iron homeostasis leading to mitochondrial iron accumulation (46,47). To determine if iron regulation is dysfunctional in *erv1* and *mia40* mutants, we measured the expression of two iron regulon genes, *FET3* and *FIT3*, under varying iron growth conditions. *FET3* encodes a multicopper oxidase involved in high affinity iron uptake, while *FIT3* encodes a cell wall mannoprotein involved in siderophore uptake (48,49). Under iron-limiting conditions, Aft1/2 induces the expression of *FET3* and *FIT3*, while under normal and high iron conditions their expression is deactivated. Using *FET3-LacZ* and *FIT3-LacZ* reporters, we measured β-galactosidase activity in extracts from cells grown in excess, normal, or limiting iron conditions. Both the *FET3* and *FIT3* reporters show misregulation of iron homeostasis in the *erv1-1* mutant (Fig. 7A,B) since the genes are highly expressed regardless of iron growth conditions. Therefore, we tested whether addition of GSH to the growth media rescued iron misregulation in this mutant. With both reporters, we saw higher overall expression compared to WT, but the pattern of expression showed functional regulation with GSH addition (lower expression when iron is normal or in excess, higher expression when iron is limiting). In addition, the other temperature-sensitive *erv1* (*erv1-2, erv1-5*) and *mia40* (*mia40-3, mia40-4*) mutants that have normal GSH levels exhibited iron regulation that was similar to the WT control under both permissive and restrictive growth temperatures (Fig. 8A). Addition of 1 mM GSH to these mutants has no effect on gene expression (data not shown). In order to show that these effects were not dependent on growth temperature, we also tested expression of the reporter genes in the *GAL-ERV1* strain. Unlike the *erv1-1* strain, *FET3* expression was decreased in Fe-deficient media with both up- and down-regulation of *ERV1* in the presence or absence of GSH. However, expression of these genes in normal and excess iron was similar to the isogenic wild-type control (Fig. 8B). A similar pattern was observed for *FIT3* expression in this strain (data not shown). Taken as a whole, these results indicate that dysfunctional iron regulation in the *erv1-1* mutant is primarily due to low levels of GSH, rather than specific defects in the Erv1 protein. Furthermore, the assays shown in Figure 8A similarly rule out a significant role for Mia40 in iron regulation.

Mitochondrial iron accumulation in erv1-1 is rescued by GSH. Previous results demonstrate that deletion or depletion of the ISC Fe-S cluster assembly or export machinery, including the glutathione-persulfide exporter Atm1, causes accumulation of iron in mitochondria (21,46,50-52). This effect is attributed to constitutive activation of the iron regulon leading to intracellular iron accumulation. To determine whether iron levels are affected by *erv1* dysfunction, iron levels in mitochondrial and cytosolic extracts were measured in several *erv1* mutants grown in SC media (normal iron levels) using atomic absorption spectroscopy (Fig. 9). Cytosolic and mitochondrial iron levels are elevated in the *erv1-1* mutant at the restrictive temperature (37 °C) by ~2.5× and ~7-8×, respectively, relative to temperature-matched WT controls (Fig. 9A,B, left panels). These results are consistent with upregulation of Aft1/2-activated genes in this strain as shown in Figure 7. Addition of 1 mM GSH rescued this high iron phenotype (Fig. 9A,B, right panels) as observed for the iron misregulation phenotype. We further measured mitochondrial and cytosolic iron levels in an *erv1(F124S)* mutant in the W303A background since a previous report suggested that mitochondrial iron is elevated in this strain (47). However, the temperature-sensitive *erv1(F124S)* mutant did not exhibit substantial changes in mitochondrial or cytosolic iron levels at 37 °C, with only 2-fold higher cytosolic iron and wild-type levels of mitochondrial iron (Fig. 9C,D, left panels). Finally, we measured subcellular iron levels in a *GAL-ERV1* strain and detected a similar trend. When Erv1 is depleted, cytosolic iron is slightly elevated (~2× WT levels), while mitochondrial iron remains similar to WT. As a positive control, we measured iron levels in a *GAL-ATM1* strain that was shown to accumulate mitochondrial iron when *ATM1* expression is turned off (21,51,53). Similar to previous results, mitochondrial iron levels were found to be 7× higher than WT when Atm1 is depleted, while cytosolic levels remained unchanged (Fig. 9C,D, left panels). Taken together, these data reaffirm that only the *erv1-1* mutant harboring a *GSH1* mutation exhibits significant defects in iron homeostasis that are rescued with exogenous GSH, and furthermore rule out an essential role for Erv1 in iron regulation.

DISCUSSION

The specific role of Erv1 in cytosolic Fe-S cluster maturation and iron signaling has been a long-standing mystery ever since Fe-S cluster defects were reported for a temperature-sensitive (ts) *erv1* strain in 2001 (7). This report is widely cited, yet no subsequent study in yeast has revisited these results to provide a molecular explanation for these observations. To address this issue, we obtained the original *erv1* ts strain (*erv1-1*) as well as additional temperature-sensitive and *GAL*-regulated *erv1* mutants in a variety of strain backgrounds. We measured the *in vivo* Mia40 redox state in each of these strains and confirmed the defect in Erv1 sulfhydryl oxidase activity at the restrictive temperature or upon Erv1 depletion. However, only the *erv1-1* strain exhibited decreased activity for the cytosolic Fe-S enzymes isopropylmalate isomerase and sulfite reductase. Since some of these defects were rescued with GSH addition to the growth media, we measured GSH levels in the *erv1* and *mia40* mutants and discovered that the *erv1-1* strain has dramatically lowered GSH levels compared to the other WT and mutant strains. By sequencing the *GSH1* gene in *erv1-1*, an R280H mutation in the glutamate cysteine ligase coding sequence was identified. Since Erv1 was also reported to impact iron regulation in addition to cytosolic Fe-S cluster maturation (8), we extended these studies to examine the effect of Erv1 and Mia40 dysfunction or depletion on iron regulation. Similar to the Fe-S enzyme activity defects, iron misregulation leading to mitochondrial iron accumulation was only detected in the GSH-depleted *erv1-1* strain. Addition of GSH to the growth media rescued the iron-dependent phenotypes in *erv1-1*, suggesting that GSH deficiency is the underlying cause rather than non-functional Erv1.

In light of the new information provided by our study, we reevaluated the results from the original 2001 *erv1* paper (7). In that publication, the authors reported that ^{55}Fe incorporation into the cytosolic Fe-S proteins Leu1 and Rli1 in *erv1-1* is ~10-30% lower than WT at 24 °C while approximately 90% lower at 37 °C. Given that GSH is also critical for maturation of cytosolic Fe-S cluster proteins (20), we suggest that these

differences in iron loading may be due to changes in GSH levels in *erv1-1* at 24 vs. 37 °C. We found that whole cell GSH levels in *erv1-1* are 80× lower than WT at 24 °C but 400× lower at 37 °C (Fig. 3A). Thus, the intracellular GSH concentration in *erv1-1* at 24 °C may provide sufficient GSH to sustain cytosolic Fe-S cluster assembly. However, at 37 °C, the GSH concentration likely drops below a critical threshold due to increased instability of the R280H Gsh1 mutant (Fig. 5A,B), leading to a defect in maturation of cytosolic Fe-S proteins. This explanation is supported by numerous studies showing that GSH must be severely depleted (levels >100× below WT) to impact cytosolic Fe-S cluster biogenesis and iron regulation (14,20), reinforcing the proposal that GSH is required in only trace amounts to function in these pathways (16).

The 2001 Lange paper also reported that expression of Erv1 or its human homologue ALR (augmenter of liver regeneration) on a plasmid restored ^{55}Fe incorporation into Leu1 (7). We note that Erv1 and ALR were both expressed from a high copy yeast episomal plasmid (*LEU2* selection for Erv1 and *URA3* selection for ALR) under the control of a constitutive promoter in that study. Leu1 Fe-S incorporation in these assays is complicated by using *LEU2* as a selectable marker for some strains and not others, since expression of *LEU2* is shown to impact Leu1 expression levels and Fe-S loading (30,31). Furthermore, Erv1 and ALR were likely overexpressed under those conditions. Interestingly, we note that constitutive overexpression of Erv1 in the *GAL-ERV1* strain (Fig. 4A) leads to a 2.8-fold increase in GSH levels (Fig. 4C). Therefore it is possible that increased Erv1/ALR expression in the previous study may have boosted the GSH concentration above the threshold required for sustain Fe-S cluster protein maturation. Pinpointing the mechanism by which increased Erv1 expression impacts GSH levels is beyond the scope of this study but will be investigated in the future.

We also investigated the possibility that Erv1 may play an indirect role in the maturation of cytosolic Fe-S proteins and iron homeostasis. Erv1 has a clear, undisputed function in facilitating import of nuclear-encoded proteins into the mitochondrial intermembrane space. Substrates of the Erv1-Mia40 import system include assembly factors and components of the respiratory chain, chaperones that facilitate protein import into mitochondrial compartments and membranes, and chaperones for antioxidant enzymes (54). Thus, it is not surprising that Erv1 dysfunction has pleotropic effects on mitochondrial biogenesis, function, and morphology. Since cytosolic Fe-S cluster biogenesis is dependent on the mitochondrial ISC pathway and Atm1 function, Erv1 dysfunction may indirectly impact synthesis and assembly of the Atm1-exported substrate (GS-S-SG) required for maturation of cytosolic Fe-S proteins and regulation of iron homeostasis. However, under our growth and assay conditions using multiple *erv1* mutants we did not detect major effects of Erv1 dysfunction on cytosolic Fe-S protein activity nor iron regulation, leading us to conclude that Erv1 does not have a direct or indirect role in these pathways. We note that our conclusions are reinforced by a recent study in human cells, demonstrating that depletion of ALR (the human Erv1 homologue) does not impact the maturation of cytosolic Fe-S proteins assembled via the CIA pathway (55).

Our results also demonstrate that Mia40, the functional partner for Erv1, has little impact on Fe-S cluster assembly and iron regulation. It was important to address this issue since previous studies have demonstrated that recombinant human and yeast Mia40 expressed in *E. coli* can be purified aerobically with a bound [2Fe-2S] cluster (56,57). Furthermore, ^{55}Fe incorporation experiments demonstrated that yeast Mia40 binds iron *in vivo* via the redox active CxC motif (57). Although the physiological function of the Fe-S cluster in Mia40 is unknown, the authors of that report speculated that Fe-S binding to Mia40 could be involved in regulating the thiol oxidoreductase activity of Mia40 or Fe-S-Mia40 may have a role in ISC biogenesis (57). Our results argue against the latter possibility since *mia40* mutants display normal Leu1 and cytosolic and mitochondrial aconitase activities and normal expression of Fe-S-dependent, Aft1/2-regulated genes.

ACKNOWLEDGEMENTS

We thank Roland Lill (Philipps-Universität, Marburg, Germany) for providing JRY-674, *erv1-1*, and *GAL-ERV1* strains, Agnieszka Chacinska (International Institute for Molecular and Cell Biology, Warsaw, Poland) for YPH499, *erv1-2*, *erv1-5*, *mia40-3*, and *mia40-4* strains, Andy Dancis (University of Pennsylvania, USA) for pRS425-IRP1, Dennis Winge (University of Utah, USA) for pFC-W, and Jan Riemer (University of Cologne, Germany) for the spore 2A strain, pYX232-*Erv1*, and anti-Mia40 and anti-Erv1 antibodies. We thank Rabindra Behera (C. Outten research group, USC) for preparation of the *erv1(F124S)* strain. We also thank Jan Riemer and Andy Dancis for technical advice. This work was supported by grants from the National Institutes of Health (GM0086619 to CEO and GM077289 to JJB) and the Biotechnology and Biological Sciences Research Council (Institute Strategic Programmes) to JB.

CONFLICT OF INTEREST

The authors declare that they have no conflicts of interest with the content of this article.

AUTHOR CONTRIBUTIONS

HKO performed GSH measurements, Mia40/Erv1/Gsh1 western blots, *GSH1* sequencing, and RT-PCR experiments. ACD performed β–galactosidase assays, in-gel aconitase assays, and subcellular iron measurements. JH performed GSH measurements and Mia40 western blots. JDT conducted the Leu1 and sulfite reductase activity assays. YL prepared the Gsh1 antibodies and the p*TEF-GSH1* plasmid. CEO, JB, and JJB supervised, conceived, and designed experiments. The manuscript was written by CEO, ACD, and HKO, and edited by JB. All authors reviewed the results and approved the final version of the manuscript.

REFERENCES

1. Herrmann, J. M., and Riemer, J. (2012) Mitochondrial disulfide relay: redox-regulated protein import into the intermembrane space. *J Biol Chem* **287**, 4426-4433
2. Sideris, D. P., and Tokatlidis, K. (2010) Oxidative protein folding in the mitochondrial intermembrane space. *Antioxid Redox Signal* **13**, 1189-1204
3. Chacinska, A., Pfannschmidt, S., Wiedemann, N., Kozjak, V., Sanjuan Szklarz, L. K., Schulze-Specking, A., Truscott, K. N., Guiard, B., Meisinger, C., and Pfanner, N. (2004) Essential role of Mia40 in import and assembly of mitochondrial intermembrane space proteins. *EMBO J* **23**, 3735-3746
4. Mesecke, N., Terziyska, N., Kozany, C., Baumann, F., Neupert, W., Hell, K., and Herrmann, J. M. (2005) A disulfide relay system in the intermembrane space of mitochondria that mediates protein import. *Cell* **121**, 1059-1069
5. Allen, S., Balabanidou, V., Sideris, D. P., Lisowsky, T., and Tokatlidis, K. (2005) Erv1 mediates the Mia40-dependent protein import pathway and provides a functional link to the respiratory chain by shuttling electrons to cytochrome c. *J Mol Biol* **353**, 937-944
6. Bihlmaier, K., Mesecke, N., Terziyska, N., Bien, M., Hell, K., and Herrmann, J. M. (2007) The disulfide relay system of mitochondria is connected to the respiratory chain. *J Cell Biol* **179**, 389-395
7. Lange, H., Lisowsky, T., Gerber, J., Mühlenhoff, U., Kispal, G., and Lill, R. (2001) An essential function of the mitochondrial sulfhydryl oxidase Erv1p/ALR in the maturation of cytosolic Fe/S proteins. *EMBO Rep* **2**, 715-720
8. Lill, R., Hoffmann, B., Molik, S., Pierik, A. J., Rietzschel, N., Stehling, O., Uzarska, M. A., Webert, H., Wilbrecht, C., and Mühlenhoff, U. (2012) The role of mitochondria in cellular iron-sulfur protein biogenesis and iron metabolism. *Biochim Biophys Acta* **1823**, 1491-1508
9. Netz, D. J., Mascarenhas, J., Stehling, O., Pierik, A. J., and Lill, R. (2014) Maturation of cytosolic and nuclear iron-sulfur proteins. *Trends Cell Biol* **24**, 303-312
10. Kispal, G., Csere, P., Prohl, C., and Lill, R. (1999) The mitochondrial proteins Atm1p and Nfs1p are essential for biogenesis of cytosolic Fe/S proteins. *EMBO J* **18**, 3981-3989
11. Schaedler, T. A., Thornton, J. D., Kruse, I., Schwarzlander, M., Meyer, A. J., van Veen, H. W., and Balk, J. (2014) A conserved mitochondrial ATP-binding cassette transporter exports glutathione polysulfide for cytosolic metal cofactor assembly. *J Biol Chem* **289**, 23264-23274
12. Srinivasan, V., Pierik, A. J., and Lill, R. (2014) Crystal structures of nucleotide-free and glutathione-bound mitochondrial ABC transporter Atm1. *Science* **343**, 1137-1140
13. Lee, J. Y., Yang, J. G., Zhitnitsky, D., Lewinson, O., and Rees, D. C. (2014) Structural basis for heavy metal detoxification by an Atm1-type ABC exporter. *Science* **343**, 1133-1136
14. Rutherford, J. C., Ojeda, L., Balk, J., Mühlenhoff, U., Lill, R., and Winge, D. R. (2005) Activation of the iron regulon by the yeast Aft1/Aft2 transcription factors depends on mitochondrial but not cytosolic iron-sulfur protein biogenesis. *J Biol Chem* **280**, 10135-10140
15. Outten, C. E., and Albetel, A. N. (2013) Iron sensing and regulation in *Saccharomyces cerevisiae*: Ironing out the mechanistic details. *Curr Opin Microbiol* **16**, 662-668
16. Kumar, C., Igbaria, A., D'Autreaux, B., Planson, A. G., Junot, C., Godat, E., Bachhawat, A. K., Delaunay-Moisan, A., and Toledano, M. B. (2011) Glutathione revisited: a vital function in iron metabolism and ancillary role in thiol-redox control. *EMBO J* **30**, 2044-2056
17. Poor, C. B., Wegner, S. V., Li, H., Dlouhy, A. C., Schuermann, J. P., Sanishvili, R., Hinshaw, J. R., Riggs-Gelasco, P. J., Outten, C. E., and He, C. (2014) Molecular mechanism and structure of the *Saccharomyces cerevisiae* iron regulator Aft2. *Proc Natl Acad Sci U S A* **111**, 4043-4048
18. Ueta, R., Fujiwara, N., Iwai, K., and Yamaguchi-Iwai, Y. (2012) Iron-induced dissociation of the Aft1p transcriptional regulator from target gene promoters is an initial event in iron-dependent gene suppression. *Mol Cell Biol* **32**, 4998-5008
19. Lisowsky, T. (1992) Dual function of a new nuclear gene for oxidative phosphorylation and vegetative growth in yeast. *Mol Gen Genet* **232**, 58-64

20. Sipos, K., Lange, H., Fekete, Z., Ullmann, P., Lill, R., and Kispal, G. (2002) Maturation of cytosolic iron-sulfur proteins requires glutathione. *J Biol Chem* **277**, 26944-26949
21. Kispal, G., Csere, P., Guiard, B., and Lill, R. (1997) The ABC transporter Atm1p is required for mitochondrial iron homeostasis. *FEBS Lett* **418**, 346-350
22. Bien, M., Longen, S., Wagener, N., Chwalla, I., Herrmann, J. M., and Riemer, J. (2010) Mitochondrial disulfide bond formation is driven by intersubunit electron transfer in Erv1 and proofread by glutathione. *Mol Cell* **37**, 516-528
23. Mumberg, D., Muller, R., and Funk, M. (1995) Yeast vectors for the controlled expression of heterologous proteins in different genetic backgrounds. *Gene* **156**, 119-122
24. Daum, G., Bohni, P. C., and Schatz, G. (1982) Import of proteins into mitochondria. Cytochrome b2 and cytochrome c peroxidase are located in the intermembrane space of yeast mitochondria. *J Biol Chem* **257**, 13028-13033
25. Outten, C. E., and Culotta, V. C. (2004) Alternative start sites in the *Saccharomyces cerevisiae GLR1* gene are responsible for mitochondrial and cytosolic isoforms of glutathione reductase. *J Biol Chem* **279**, 7785-7791
26. Hu, J., Dong, L., and Outten, C. E. (2008) The redox environment in the mitochondrial intermembrane space is maintained separately from the cytosol and matrix. *J Biol Chem* **283**, 29126-29134
27. Biterova, E. I., and Barycki, J. J. (2009) Mechanistic details of glutathione biosynthesis revealed by crystal structures of *Saccharomyces cerevisiae* glutamate cysteine ligase. *J Biol Chem* **284**, 32700-32708
28. Livak, K. J., and Schmittgen, T. D. (2001) Analysis of relative gene expression data using real-time quantitative PCR and the 2(-Delta Delta C(T)) Method. *Methods* **25**, 402-408
29. Tong, W. H., and Rouault, T. A. (2006) Functions of mitochondrial ISCU and cytosolic ISCU in mammalian iron-sulfur cluster biogenesis and iron homeostasis. *Cell Metab* **3**, 199-210
30. Bedekovics, T., Li, H., Gajdos, G. B., and Isaya, G. (2011) Leucine biosynthesis regulates cytoplasmic iron-sulfur enzyme biogenesis in an Atm1p-independent manner. *J Biol Chem* **286**, 40878-40888
31. Philpott, C. C., Leidgens, S., and Frey, A. G. (2012) Metabolic remodeling in iron-deficient fungi. *Biochim Biophys Acta* **1823**, 1509-1520
32. Yamaguchi-Iwai, Y., Stearman, R., Dancis, A., and Klausner, R. D. (1996) Iron-regulated DNA binding by the AFT1 protein controls the iron regulon in yeast. *EMBO J* **15**, 3377-3384
33. Rutherford, J. C., Jaron, S., and Winge, D. R. (2003) Aft1p and Aft2p mediate iron-responsive gene expression in yeast through related promoter elements. *J Biol Chem* **278**, 27636-27643
34. Thorvaldsen, J. L., Sewell, A. K., McCowen, C. L., and Winge, D. R. (1993) Regulation of metallothionein genes by the ACE1 and AMT1 transcription factors. *J Biol Chem* **268**, 12512-12518
35. Lisowsky, T. (1994) ERV1 is involved in the cell-division cycle and the maintenance of mitochondrial genomes in *Saccharomyces cerevisiae*. *Curr Genet* **26**, 15-20
36. Guo, P. C., Ma, J. D., Jiang, Y. L., Wang, S. J., Bao, Z. Z., Yu, X. J., Chen, Y., and Zhou, C. Z. (2012) Structure of yeast sulfhydryl oxidase erv1 reveals electron transfer of the disulfide relay system in the mitochondrial intermembrane space. *J Biol Chem* **287**, 34961-34969
37. Muller, J. M., Milenkovic, D., Guiard, B., Pfanner, N., and Chacinska, A. (2008) Precursor oxidation by Mia40 and Erv1 promotes vectorial transport of proteins into the mitochondrial intermembrane space. *Mol Biol Cell* **19**, 226-236
38. Hofhaus, G., Lee, J. E., Tews, I., Rosenberg, B., and Lisowsky, T. (2003) The N-terminal cysteine pair of yeast sulfhydryl oxidase Erv1p is essential for in vivo activity and interacts with the primary redox centre. *Eur J Biochem* **270**, 1528-1535
39. Rissler, M., Wiedemann, N., Pfannschmidt, S., Gabriel, K., Guiard, B., Pfanner, N., and Chacinska, A. (2005) The essential mitochondrial protein Erv1 cooperates with Mia40 in biogenesis of intermembrane space proteins. *J Mol Biol* **353**, 485-492

40. Yarunin, A., Panse, V. G., Petfalski, E., Dez, C., Tollervey, D., and Hurt, E. C. (2005) Functional link between ribosome formation and biogenesis of iron-sulfur proteins. *EMBO J* **24**, 580-588
41. Hausmann, A., Aguilar Netz, D. J., Balk, J., Pierik, A. J., Mühlenhoff, U., and Lill, R. (2005) The eukaryotic P loop NTPase Nbp35: an essential component of the cytosolic and nuclear iron-sulfur protein assembly machinery. *Proc Natl Acad Sci U S A* **102**, 3266-3271
42. Zhang, Y., Lyver, E. R., Nakamaru-Ogiso, E., Yoon, H., Amutha, B., Lee, D. W., Bi, E., Ohnishi, T., Daldal, F., Pain, D., and Dancis, A. (2008) Dre2, a conserved eukaryotic Fe/S cluster protein, functions in cytosolic Fe/S protein biogenesis. *Mol Cell Biol* **28**, 5569-5582
43. Amutha, B., Gordon, D. M., Gu, Y., Lyver, E. R., Dancis, A., and Pain, D. (2008) GTP is required for iron-sulfur cluster biogenesis in mitochondria. *J Biol Chem* **283**, 1362-1371
44. Roy, A., Solodovnikova, N., Nicholson, T., Antholine, W., and Walden, W. E. (2003) A novel eukaryotic factor for cytosolic Fe-S cluster assembly. *EMBO J* **22**, 4826-4835
45. Terziyska, N., Grumbt, B., Bien, M., Neupert, W., Herrmann, J. M., and Hell, K. (2007) The sulfhydryl oxidase Erv1 is a substrate of the Mia40-dependent protein translocation pathway. *FEBS Lett* **581**, 1098-1102
46. Lill, R., Srinivasan, V., and Mühlenhoff, U. (2014) The role of mitochondria in cytosolic-nuclear iron-sulfur protein biogenesis and in cellular iron regulation. *Curr Opin Microbiol* **22**, 111-119
47. Aloria, K., Schilke, B., Andrew, A., and Craig, E. A. (2004) Iron-induced oligomerization of yeast frataxin homologue Yfh1 is dispensable in vivo. *EMBO Rep* **5**, 1096-1101
48. Askwith, C., Eide, D., Van Ho, A., Bernard, P. S., Li, L., Davis-Kaplan, S., Sipe, D. M., and Kaplan, J. (1994) The *FET3* gene of *S. cerevisiae* encodes a multicopper oxidase required for ferrous iron uptake. *Cell* **76**, 403-410
49. Philpott, C. C., Protchenko, O., Kim, Y. W., Boretsky, Y., and Shakoury-Elizeh, M. (2002) The response to iron deprivation in *Saccharomyces cerevisiae*: expression of siderophore-based systems of iron uptake. *Biochem Soc Trans* **30**, 698-702
50. Chen, O. S., Crisp, R. J., Valachovic, M., Bard, M., Winge, D. R., and Kaplan, J. (2004) Transcription of the yeast iron regulon does not respond directly to iron but rather to iron-sulfur cluster biosynthesis. *J Biol Chem* **279**, 29513-29518
51. Miao, R., Kim, H., Koppolu, U. M., Ellis, E. A., Scott, R. A., and Lindahl, P. A. (2009) Biophysical characterization of the iron in mitochondria from Atm1p-depleted *Saccharomyces cerevisiae*. *Biochemistry* **48**, 9556-9568
52. Miao, R., Martinho, M., Morales, J. G., Kim, H., Ellis, E. A., Lill, R., Hendrich, M. P., Munck, E., and Lindahl, P. A. (2008) EPR and Mossbauer spectroscopy of intact mitochondria isolated from Yah1p-depleted Saccharomyces cerevisiae. *Biochemistry* **47**, 9888-9899
53. Balk, J., Pierik, A. J., Netz, D. J., Mühlenhoff, U., and Lill, R. (2004) The hydrogenase-like Nar1p is essential for maturation of cytosolic and nuclear iron-sulphur proteins. *EMBO J* **23**, 2105-2115
54. Fischer, M., and Riemer, J. (2013) The mitochondrial disulfide relay system: roles in oxidative protein folding and beyond. *Int J Cell Biol* **2013**, 742923
55. Ferecatu, I., Goncalves, S., Golinelli-Cohen, M. P., Clemancey, M., Martelli, A., Riquier, S., Guittet, E., Latour, J. M., Puccio, H., Drapier, J. C., Lescop, E., and Bouton, C. (2014) The diabetes drug target MitoNEET governs a novel trafficking pathway to rebuild an Fe-S cluster into cytosolic aconitase/iron regulatory protein 1. *J Biol Chem* **289**, 28070-28086
56. Daithankar, V. N., Farrell, S. R., and Thorpe, C. (2009) Augmenter of liver regeneration: substrate specificity of a flavin-dependent oxidoreductase from the mitochondrial intermembrane space. *Biochemistry* **48**, 4828-4837
57. Spiller, M. P., Ang, S. K., Ceh-Pavia, E., Fisher, K., Wang, Q., Rigby, S. E., and Lu, H. (2013) Identification and characterization of mitochondrial Mia40 as an iron-sulfur protein. *Biochem J* **455**, 27-35
58. Sikorski, R. S., and Hieter, P. (1989) A system of shuttle vectors and yeast host strains designed for efficient manipulation of DNA in *Saccharomyces cerevisiae*. *Genetics* **122**, 19-27

FIGURE LEGENDS

Figure 1. Mia40 redox state in *erv1* temperature-sensitive mutants. Redox state of Mia40 measured in whole cell extracts from the indicated *erv1* mutants and WT controls grown at permissive (24 °C) or restrictive temperatures (37 °C) in SC glucose media. WT(1): JRY-675, WT(2): YPH499. TCA-precipitated extracts were resuspended in loading buffer with NEM, separated by non-reducing SDS-PAGE, and immunoblotted against Mia40. Reduced (red) and oxidized (ox) forms of Mia40 were quantified using an Odyssey Infrared Imaging System. Representative Mia40 redox western blots are shown above graphs. Data shown are means + S.D. for 3-6 independent experiments. Cartoon depicts reduced and oxidized forms of Mia40.

Figure 2. Activity of Fe-S enzymes in *erv1* and *mia40* mutants. ***A***, Leu1 (isopropylmalate isomerase) activity for the indicated strains compared to isogenic WT controls grown in SD glucose media after shifting to 37 °C for 5 hrs. Data shown are means + S.D. for 3 independent experiments. ***B,*** Western blots of whole cell extracts from WT, *erv1*, and *nbp35-1* strains immunoblotted against Leu1. Cells were grown at 37 °C in SC glucose media for 5 hrs with or without the addition of 1 mM GSH as indicated. ***C*****,** Indirect assay for sulfite reductase activity. Serial dilutions of WT (JRY-675) and *erv1-1* strains were plated on SD bismuth-sulfite plates with or without the addition of 1 mM GSH. Cell grown on SD plates without bismuth are shown on the left (-Bi). *Top*, Against white background to show brown color as a result of the accumulation of sulfide product; *Bottom*, Against dark background to show yeast growth. (***D-E***) *Top*, In-gel aconitase activity assays for (***D***) JRY-675 (WT(1)) and *erv1-1*, and (***E***) YPH499 (WT(2)) and isogenic *erv1* and *mia40* mutant strains expressing human IRP1 (pRS425-IRP1). C: WT control strain without human IRP1 expression plasmid. Cells were grown in SC glucose media with or without the addition of 1 mM GSH as indicated. Mitochondrial (Aco1) and cytosolic aconitase (IRP1) run separately in native gels. *Bottom*, The same protein extracts were separated by reducing SDS-PAGE and immunoblotted against human IRP1 and yeast Pgk1 (loading control).

Figure 3. GSH and Erv1 protein levels in *erv1* and *mia40* temperature-sensitive mutants. (***A***) Whole cell, (***B***) cytosolic, and (***C***) mitochondrial GSH levels in WT, *erv1*, and *mia40* temperature-sensitive mutants grown at 24 and 37 °C in SC glucose media. Data shown are means + S.D. for 3-12 independent experiments. ***D,*** Mitochondrial extracts (20 µg) from WT, *erv1*, and *mia40* mutant strains separated by reducing SDS-PAGE and immunoblotted against Erv1 and Porin (loading control). Cells were grown at 24 °C or 37 °C in SC glucose media.

Figure 4. Mia40 redox state and GSH levels in *erv1(F124S)* and *GAL-ERV1* strains. ***A***, (*top*) Mia40 redox state in whole cell extracts determined by non-reducing SDS-PAGE and immunoblotting as described in Fig. 1. *Left panel*, WT (W303A-*ERV1*) and *erv1(F124S)* strains grown at 24 or 37 °C in SC glucose media. *Right panel*, WT (W303A) and *GAL-ERV1* strains grown in SC raffinose/galactose media (*GAL* promoter ON) or in SC raffinose media for 64 hrs (*GAL* promoter OFF). (*Bottom*) Mitochondrial extracts (20 µg) from WT and *GAL-ERV1* strains separated by reducing SDS-PAGE and immunoblotted against Erv1 and Porin (loading control) demonstrate overexpression or depletion of Erv1 in the ON and OFF modes. ***B***, Quantification of Mia40 redox western blots from *A*. ***C***, GSH levels measured in whole cell extracts as described in Fig. 3. In ***B*** and ***C***, data shown are means + S.D. for 3-12 independent experiments.

Figure 5. Gsh1 protein levels are dramatically decreased in *erv1-1* due to a mutation in *GSH1*. ***A***, Western blots of PMS extracts (75 µg) from WT, *erv1*, and *mia40* mutant strains immunoblotted against Gsh1 and Pgk1 (loading control). WT(1): JRY-675, WT(2): YPH499. ***B,*** Gsh1 proteins levels quantified from western blots in (***A***) are shown relative to the Pgk1 loading control and normalized to isogenic WT strains. ***C,*** Quantitative RT-PCR results for *GSH1* mRNA levels in WT (JRY-675) and *erv1-1* strains grown in SD glucose media at 24 and 37 °C. Fold change in *GSH1* mRNA levels is shown relative to

ACT1 control and normalized to WT cells at 24 °C (set as 1.0). ***D***, Amino acid sequence comparison of glutamate cysteine ligase (Gsh1) orthologs from *S. cerevisiae* (UniProtKB:P32477), *S. pombe* (Q09768), *D. melanogaster* (Q9W3K5), mouse (P97494), and human (P48506) aligned using ClustalW2. Identical residues are highlighted in blue and similar residues in yellow. Arg-280 from *S. cerevisiae* Gsh1 is shown with an arrow in pink, which is mutated to a His in the *erv1-1* strain. ***E***, Crystal structure of *S. cerevisiae* Gsh1 (PDB 3IG8) displayed as a cartoon model. The glutamate substrate (yellow and atom colors) and ADP (orange and atom colors) are shown in ball and stick representation and Mg^{2+} ions are shown as cyan spheres. Side chains for Arg-280 and Asp-403 are shown in pink and green, respectively, with the salt bridge shown as black lines. The Y362-G370 loop that is likely disturbed by the R280H mutation is shown in red. In ***B*** and ***C*****,** data shown are means + S.D. for 3 independent experiments.

Figure 6. Defects in *erv1-1* GSH metabolism are rescued with expression of WT *GSH1* or GSH addition to the growth media. ***A***, PMS extracts (75 µg) from WT (JRY-675), *erv1-1*, and *erv1-1* transformed with pRS415 (vector) or pTEF-GSH1 (p*GSH1*) separated by non-reducing SDS-PAGE and immunoblotted against Gsh1 and Pgk1 (loading control). ***B***, Whole cell GSH levels in WT, *erv1-1*, and *erv1-1* transformed with p*TEF-GSH1* (+ pGSH1) grown at 24 and 37 °C in SC glucose media. + GSH indicates the addition of 1 mM GSH to the growth media in these samples. Data shown are means + S.D. for 3-10 independent experiments.

Figure 7. Iron regulation is disrupted in *erv1-1* but rescued with GSH addition. β-galactosidase activity assays were performed for JRY-675 (WT(1)) and *erv1-1* strains expressing a (***A***) *FET3-LacZ* or (***B***) *FIT3-LacZ* reporter plasmid grown in SC media with excess, normal, or deficient Fe levels with or without addition of 1 mM GSH as indicated. Data shown are means + S.D. for 3-6 independent experiments.

Figure 8. Iron regulation in *erv1* and *mia40* mutants with normal GSH levels is not disrupted. β-galactosidase activity assays were performed for strains expressing a *FET3-LacZ* reporter plasmid grown in SC media with excess, normal, or deficient Fe levels. Data shown are means + S.D. for 3-6 independent experiments. Strains tested were (***A***) YPH499 (WT(2)) and *erv1-2, erv1-5, mia40-3, mia40-4*, and (***B***) W303A (WT(3)) and *GAL-ERV1*.

Figure 9. Subcellular iron accumulation in *erv1* strains. Cytosolic (***A***) and mitochondrial (***B***) iron levels in WT and *erv1-1* strains grown in SC media with or without addition of 1 mM GSH as indicated. WT(1): JRY-675. Cytosolic (***C***) and mitochondrial (***D***) iron levels in WT, *erv1(F124S), GAL-ERV1*, and *GAL-ATM1* strains grown in SC media. WT(2): W303A-*ERV1*, WT(3): W303A. Data shown are means + S.D. for 3 independent experiments.

TABLES

Table 1. Strains used in this study

Strain	Genotype	Reference
JRY-675	*MAT*a, Δ*leu2, ura3-52, his4-519*	(19)
erv1-1 (*pet492-6A*)	*MAT*a, Δ*leu2, ura3-52, pet492*^{ts}	(19)
YPH499	*MAT*a, *ade2-101*, *his3-Δ200*, *leu2-Δ1*, *ura3-52*, *trp1-Δ63*, *lys2-801*	(58)
erv1-2	*MAT*a, *ade2-101*, *his3-Δ200*, *leu2-Δ1*, *ura3-52*, *trp1-Δ63*, *lys2-801*, *erv1::ADE2* [pFL39-*erv1-2*]	(39)
erv1-5	*MAT*a, *ade2-101*, *his3-Δ200*, *leu2-Δ1*, *ura3-52*, *trp1-Δ63*, *lys2-801*, *erv1::ADE2* [pFL39-*erv1*-C159S]	(37)
mia40-3	*MAT*a, *ade2-101*, *his3- Δ200*, *leu2-Δ1*, *ura3-52*, *trp1-Δ63*, *lys2-801*, *mia40::ADE2* [pFL39-*mia40-3*]	(3)
mia40-4	*MAT*a, *ade2-101*, *his3-Δ200*, *leu2-Δ1*, *ura3-52*, *trp1-Δ63*, *lys2-801*, *mia40::ADE2* [pFL39-*mia40-4*]	(3)
W303A	*MAT*a, *ade2-1, his3-11,15, leu2-3,112, trp1-1, ura3-1*, *can1-100*	
GAL-ERV1	*MAT*a, *ade2-1, his3-11,15, leu2-3,112, trp1-1, ura3-1*, *can1-100, pERV1::GALL-natNT2*	R. Lill, unpublished
GAL-ATM1	*MAT*a, *ade2-1, his3-11,15, leu2-3,112, trp1-1, ura3-1*, *can1-100, pATM1::GAL10-LEU2*	(10)
Spore 2A (W303)	*MAT*a, *ade2-1, his3-11,15, leu2-3,112, trp1-1, ura3-1, can1-100 erv1::HIS3* [p*ERV1*(URA3)]	(22)
W303-*ERV1*	*MAT*a, *ade2-1, his3-11,15, leu2-3,112, trp1-1, ura3-1, can1-100 erv1::HIS3* [pYX232-*ERV1*]	This study
W303-*erv1(F124S)*	*MAT*a, *ade2-1, his3-11,15, leu2-3,112, trp1-1, ura3-1, can1-100 erv1::HIS3* [pYX232-*erv1(F124S)*]	This study
BY4741	*MAT*a, *his3Δ1*, *leu2Δ0*, *met15Δ0*, *ura3Δ0*	
npb35-1	*MAT*a, *his3Δ1*, *leu2Δ0*, *met15Δ0*, *ura3Δ0*, *nbp35::kanMX4* [pRS315-*nbp35-1*]	(40)

Table 2. Primers used for sequencing and qRT-PCR.

Primer Name	Primer Sequence
***GSH1* Sequencing Primers**	
GSH1 -700	5′-GTTTGGTTCAGCGCGACGAG-3′
GSH1 term	5′-CAGGAGATTCCAGGTTCGAG-3′
GSH1 seq forward	5′-GCTAGCCGACCAAGATGTTC-3′
GSH1 seq reverse	5′-CAATGCCTCCAAATCCGTTC-3′
qRT-PCR Primers	
GSH1 forward	5′- TCTAGGACGTACAATGAACAC-3′
GSH1 reverse	5′- CCTCCATATTAAGCTCAGTG -3′
ACT1 forward	5′- GGATTCCGGTGATGGTGTTACT -3′
ACT1 reverse	5′- TGGCGTGAGGTAGAGAGAAACC-3′

Figure 1.

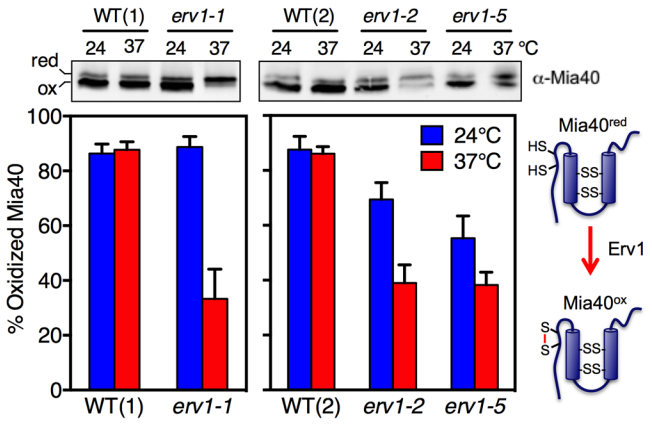

Figure 2.

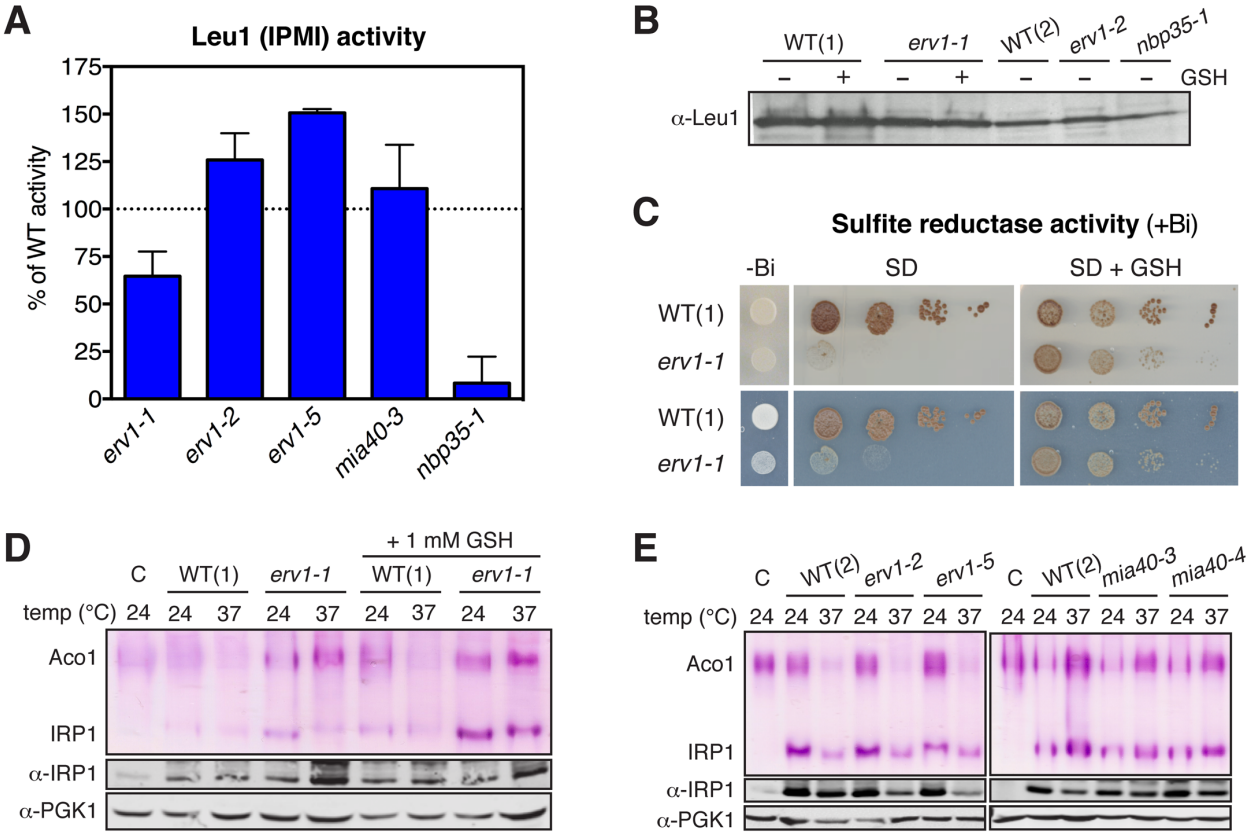

Figure 3.

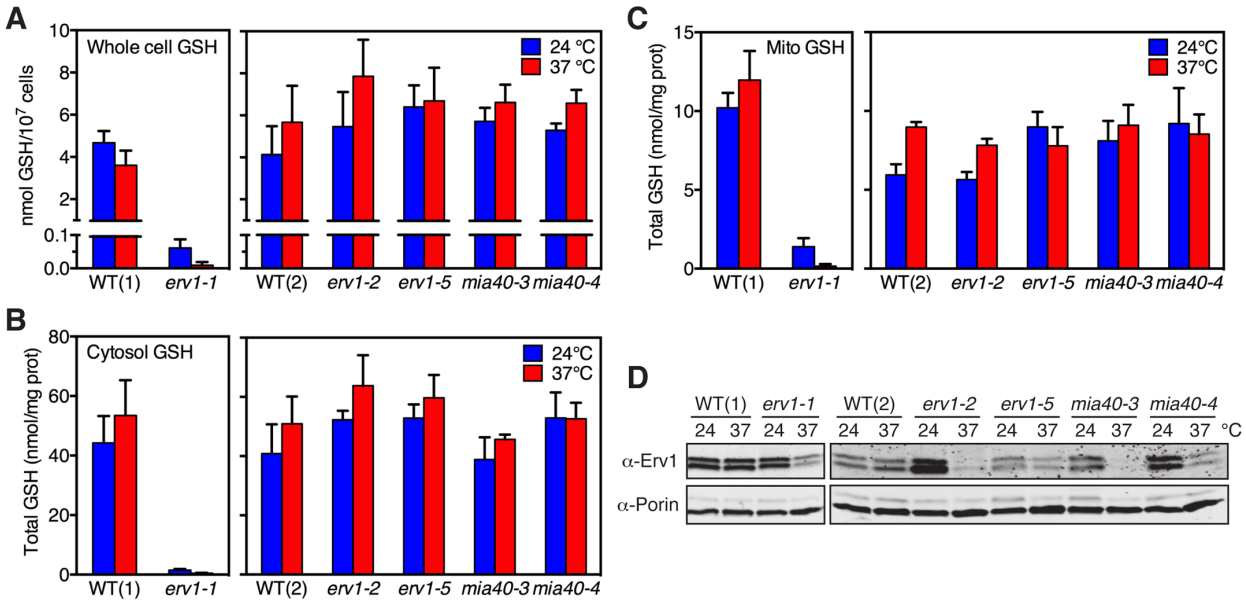

Figure 4.

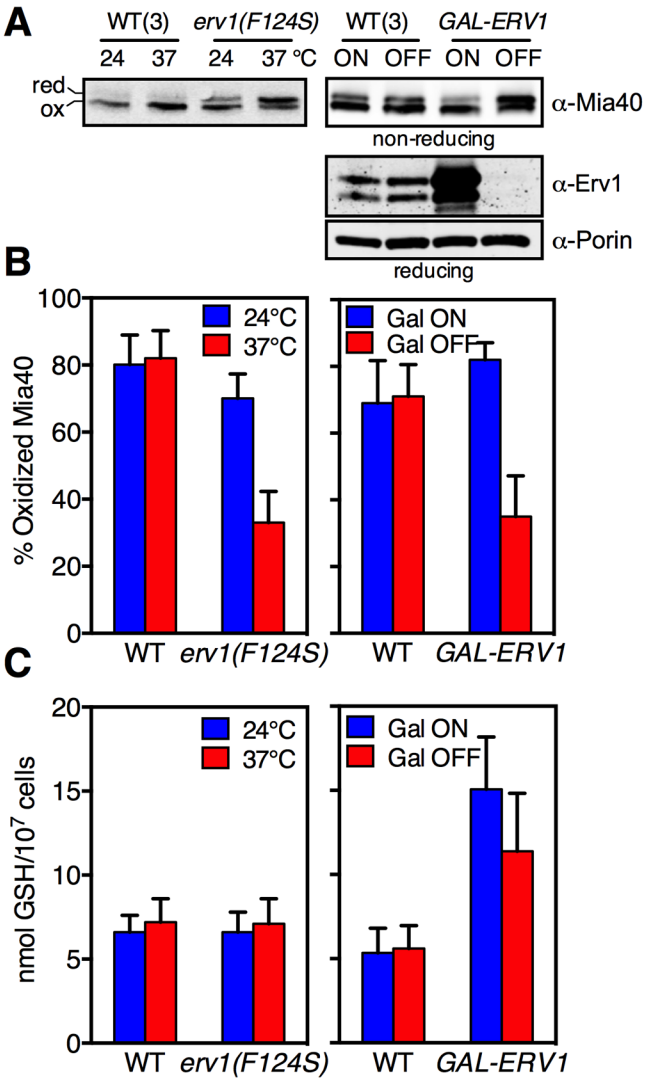

Figure 5.

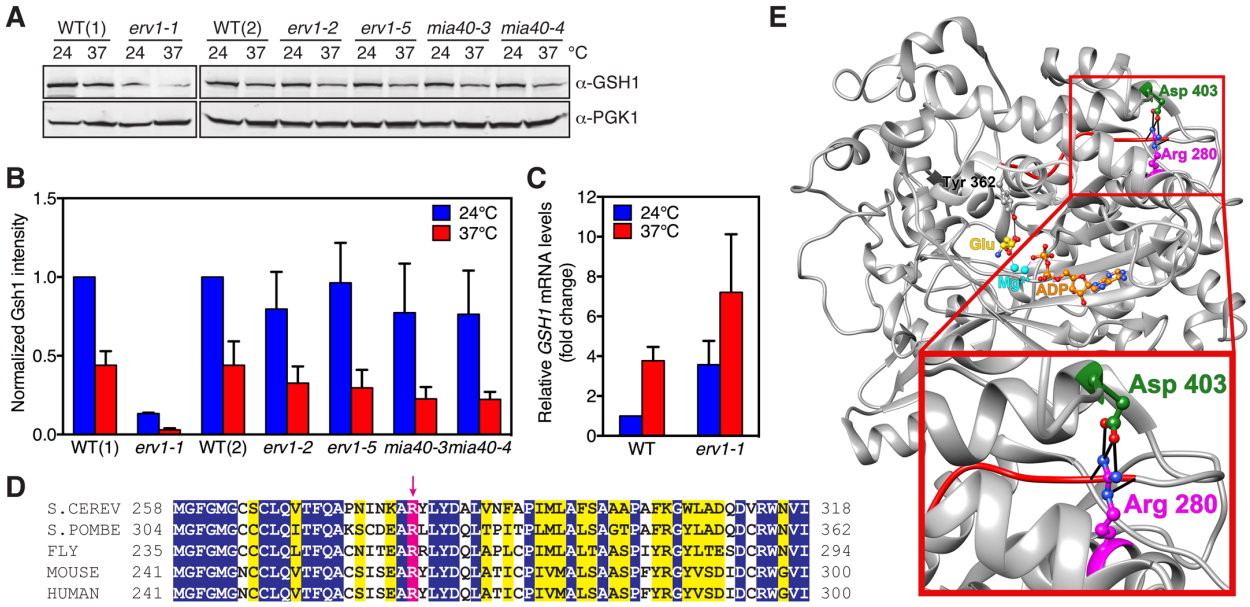

Figure 6.

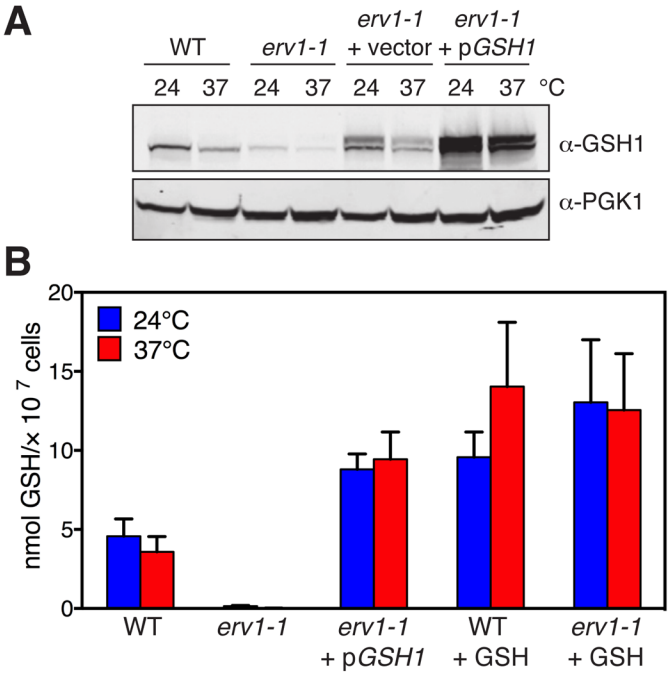

Figure 7.

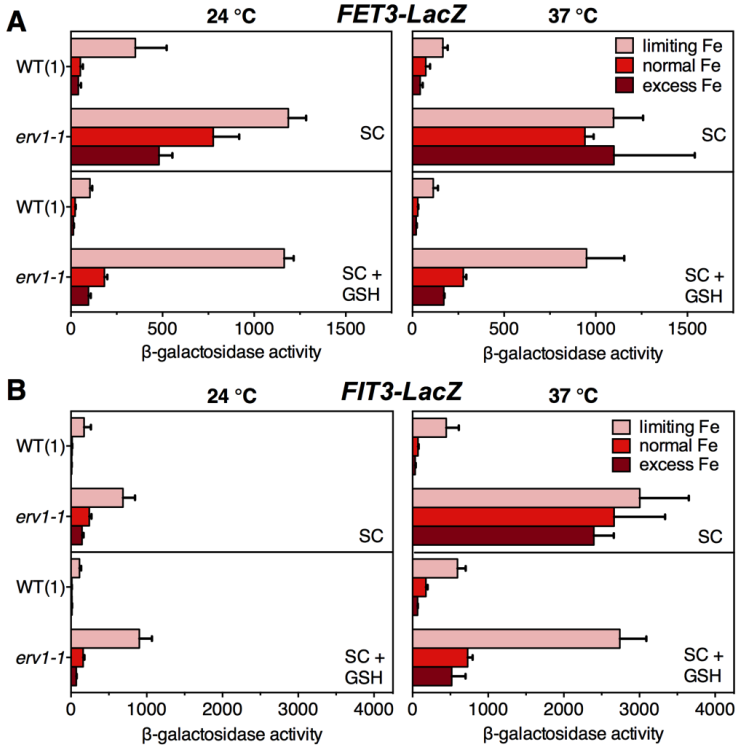

Figure 8.

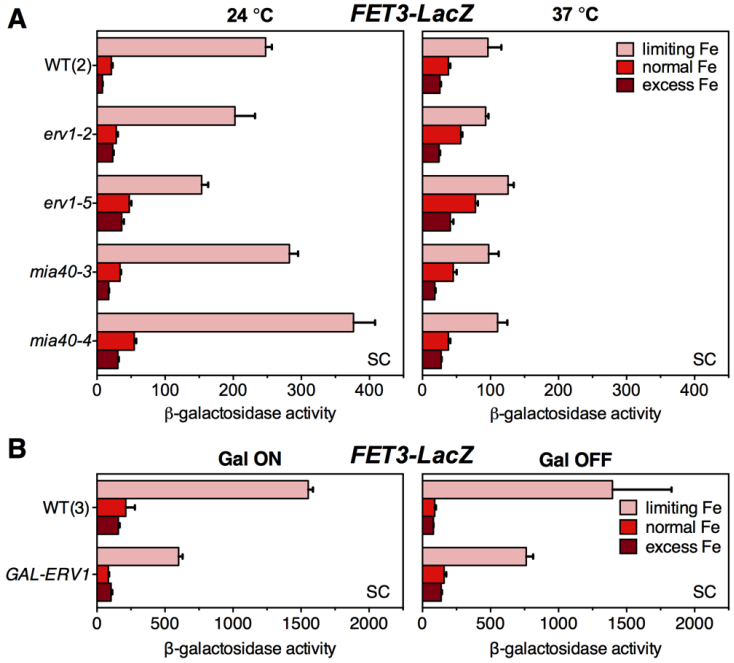

Figure 9.

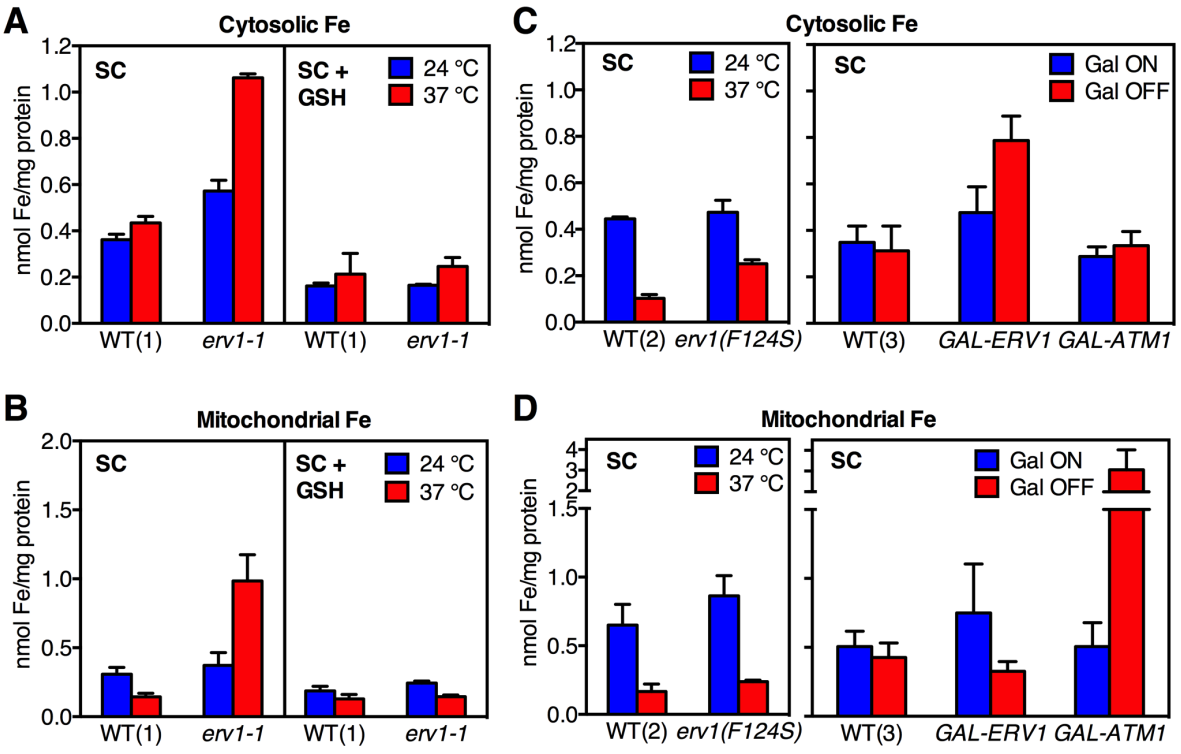

Gene Regulation:

Cytosolic Fe-S Cluster Protein Maturation and Iron Regulation Are Independent of the Mitochondrial Erv1/Mia40 Import System

Hatice K. Ozer, Adrienne C. Dlouhy, Jeremy D. Thornton, Jingjing Hu, Yilin Liu, Joseph J. Barycki, Janneke Balk and Caryn E. Outten

J. Biol. Chem. published online September 22, 2015

Access the most updated version of this article at doi: 10.1074/jbc.M115.682179